Archean to early Paleoproterozoic iron formations document a transition in iron oxidation mechanisms

Changle Wang, Leslie Robbins, Noah Planavsky, Nicolas Beukes, Laureline Patry, Stefan Lalonde, Maxwell Lechte, Dan Asael, Christopher Reinhard, Lianchang Zhang, et al.

Archean to early Paleoproterozoic iron formations document a transition in iron oxidation mechanisms

Changle Wang[1,2,3,*], Leslie J. Robbins[2,4*], Noah J. Planavsky[2], Nicolas J. Beukes[6], Laureline A. Patry[7], Stefan V. Lalonde[7], Maxwell A. Lechte[8], Dan Asael[2], Christopher T. Reinhard[9], Lianchang Zhang[1,3], Kurt O. Konhauser[5]

[1]Key Laboratory of Mineral Resources, Institute of Geology and Geophysics, Chinese Academy of Sciences, Beijing, China.
[2]Department of Earth and Planetary Sciences, Yale University, New Haven, U.S.A.
[3]University of Chinese Academy of Sciences, Beijing, China.
[4]Department of Geology, University of Regina, Regina, SK, Canada.
[5]Department of Earth and Atmospheric Sciences, University of Alberta, Edmonton, Canada.
[6]DST-NRF CIMERA, Department of Geology, University of Johannesburg, South Africa.
[7]European Institute for Marine Studies, CNRS-UMR6538 Laboratoire Géosciences Océan, Technopôle Brest-Iroise, Plouzané, France.
[8]Department of Earth and Planetary Sciences, McGill University, Montréal, Canada.
[9]School of Earth and Atmospheric Sciences, Georgia Institute of Technology, Atlanta, U.S.A.

*Corresponding authors: Changle Wang, Leslie Robbins

Email: wangcl@mail.iggcas.ac.cn; Leslie.Robbins@uregina.ca

Abstract

It is generally accepted that photosynthetic marine planktonic bacteria were responsible for the oxidation of dissolved ferrous iron (Fe(II)) and the subsequent deposition of iron formations (IFs) throughout the Archean and early Paleoproterozoic. However, the relative roles of the different biological Fe oxidation mechanisms in driving IF deposition—such as anoxygenic photosynthesis (photoferrotrophs) and oxygenic photosynthesis (cyanobacteria)—remain poorly resolved. Here, we present coupled bulk-rock Fe isotope and manganese (Mn) versus Fe ratios from Archean to early Paleoproterozoic IFs in order to provide a new perspective on Earth's early redox history and processes leading to IF deposition. Based on this updated IF geochemical record, we bolster the case that the partial oxidation of Fe(II) to Fe(III) was central to IF genesis, arguing against extensive water column Fe(II) silicate formation as the main process driving IF deposition. The geochemistryof IFs deposited prior to the Great Oxidation Event (GOE) shows that partial Fe(II) oxidation was a common feature in either anoxic or low oxygen (O_2) conditions, where metabolic Fe(II) oxidation by photoferrotrophs is likely to have prevailed over ambient Fe(II)

oxidation by O_2 produced by cyanobacteria. Assuming that cyanobacteria evolved in the Archean, the presence of partial Fe(II) oxidation suggests that O_2 production was relatively muted during this time. This points to a model for Archean surface redox conditions, whereby oxygen oases were relatively limited in extent, likely due to low primary productivity of cyanobacteria and high Fe fluxes. We further demonstrate a gradual displacement of metabolic Fe(II) oxidation in the Archean by quantitative O_2-driven Fe(II) oxidation during the GOE by ca. 2.31 Ga.

Introduction

The atmosphere during the first half of Earth's 4.5-billion-year (Ga) history was essentially devoid of free oxygen (O_2), with atmospheric abundances less than 0.001% of the present atmospheric level (PAL) [1, 2]. Geological and geochemical constraints reveal that the first permanent rise in the partial pressure of atmospheric O_2 (pO_2) occurred between ~2.5 and 2.3 Ga, a period that has been termed the Great Oxidation Event (GOE) [3, 4, 5, 6, 7, 8]. Despite widespread agreement on these general trends, the tempo and mode of Earth's early oxygenation, and the redox conditions leading up to the GOE, remain poorly understood as few redox proxies are sufficiently precise to track secular variations in ocean-atmosphere O_2 abundance. Although incipient oxygenation of Earth's surface environments before GOE has commonly been proposed [9, 10, 11], there still remains an active debate regarding the exact timing of the first emergence of oxygenic photosynthesis [12, 13], with suggestions that this biological innovation may have coincided with the oxygenation of the atmosphere [12, 14]. Although, a recent phylogenomic study on enzymes that either produce or utilize oxygen points to an Archean origin for oxygenic photosynthesis [15]. In much the same manner, various geochemical proxies likely have different sensitivities to changes in pO_2 and may not respond uniformly [9, 10], further blurring the history of atmospheric and oceanic pO_2 as well as the exact timing of the GOE. This obscurity in the onset and timing of Earth's early oxidation has also given rise to recent questions as to what role biological oxidation played, if any, in the deposition of iron formations (IFs).

Iron formations are particularly useful sedimentary archives for tracking Fe sources and sinks during much of the Archean and early Paleoproterozoic as they formed in a range of depositional settings on the continental shelves of existing cratons [16, 17]. Moreover, because IF are chemical sediments, they represent an archive of environmental conditions and seawater composition at the time of their deposition [17], which in turn, provides insights into the availability of trace-element nutrients to, and the activity of, the ancient biosphere [18].

The best-preserved IF successions have a remarkably uniform mineralogy, composed mostly of chert, magnetite, and hematite, with variable amounts of Fe-rich silicate minerals (e.g., greenalite), carbonate minerals (e.g., siderite), and locally sparse sulfides (e.g., pyrite). It is also apparent that none of the minerals

in IFs today are primary in origin, and that the original seafloor precipitate mineralogy was not preserved. Instead, the observed minerals reflect multiple post-depositional alteration processes that modified the primary precipitates which are generally believed to have been ferric oxyhydroxides (e.g., ferrihydrite) and amorphous silica [17] (see *Supplementary Materials* for a detailed discussion on the primary mineralogy of IF).

The presence of ferric iron (Fe(III)) minerals in IFs is generally ascribed to the metabolic activity of planktonic bacteria in the photic zone of Earth's ancient oceans. The classic model invokes Fe(III) precipitation occurring at the interface between oxygenated shallow waters and reduced upwelling ferrous iron (Fe(II))-rich waters, the oxygen (O_2) being sourced from cyanobacteria, or their predecessors [19]. These photoautotrophs would have flourished when nutrients were available and passively induced the precipitation of Fe(III)-oxyhydroxide through the excretion of their metabolic waste (i.e. O_2). Alternatively, anoxygenic photoautotrophic Fe(II)-oxidizing bacteria (known as photoferrotrophs) could have directly oxidized Fe(II) and coupled this to the fixation of carbon utilizing light energy [20]. From a mass balance perspective, either metabolism could account for all the Fe(III) deposited in BIF [21, 22]. The classical view, however, has recently been challenged, with the suggestion that IFs were largely deposited as Fe(II) silicates (see [23]), a model which would negate the need for oxygenic or anoxygenic photosynthesis in IF deposition. Inspired by the apparent necessity for biologically driven redox reactions and IF precipitation, and its potential to provide insights into the oxygenation of Earth in the lead-up to the GOE, here we explore the coupled proxies of Fe isotope and manganese (Mn) to Fe ratios in an effort to better understand the link between IF deposition and the rise of oxygenic photosynthesis during the Archean and Paleoproterozoic.

Iron Formation Deposition and Marine Oxygen Levels

As Fe in seawater is soluble under anoxic conditions as Fe(II) and is rendered poorly soluble under oxic conditions, precipitating readily as Fe(III) oxyhydroxides, the secular record of Fe oxidation may potentially be leveraged to track surface O_2 levels [4, 24]. One potential means by which we can parse the mechanisms underpinning Fe(II) oxidation in the ancient oceans is through measurement of the relative abundances of

100 the different stable isotopes of Fe in the Fe-oxides of IFs [24]. This approach is appealing since the kinetics
101 of Fe(II) oxidation are well-constrained and the Fe isotope systematics of Fe(II) oxidation by
102 photoferrotrophs and ambient O_2 are relatively well-understood [25, 26, 27, 28]. Briefly, partial oxidation of
103 dissolved Fe(II) produces Fe(III)-oxyhydroxides that are enriched in ^{56}Fe, typically by 1 to 3‰, leaving the
104 residual dissolved Fe(II) ^{56}Fe-depleted, although more rapid oxidation effectively lowers this overall
105 fractionation [27]. This contrasts with the formation of reduced iron phases (e.g., Fe carbonates and silicates):
106 these pathways are typically considered to involve either a negligible fractionation or a small negative
107 fractionation [26, 27], leaving residual dissolved Fe(II) slightly ^{56}Fe-enriched. Furthermore, when Fe(II)
108 oxidation is complete and quantitative—where there is a sharp redoxcline and a well-oxygenated surface
109 layer—there is no net fractionation during the formation of Fe(III) oxides [25]. However, the fractionation
110 factors of Fe isotopes for Fe(II) oxidation by free O_2 and anoxygenic photosynthesis effectively overlap [29],
111 making it difficult to clearly recognize the mechanism responsible for Fe(II) oxidation at different points in
112 Earth's history based on solely Fe isotopes. To address this shortcoming, a supplementary record that can
113 be directly tied to Fe(II) oxidation is required.
114
115 Similar to Fe, manganese (Mn) is redox-sensitive and soluble under anoxic conditions. The oxidation of
116 Mn(II) and the subsequent formation of Mn(III/IV) oxides (from herein simply referred to as Mn oxides) in
117 the presence of free O_2 generally requires both higher redox potentials than the oxidation of Fe(II) and the
118 catalyzing activity of a Mn(II)-oxidizing bacteria [30]. Manganese oxides would also be expected to undergo
119 rapid reductive dissolution in anoxic, Fe(II)-rich seawater. As such, Mn enrichments resulting from either
120 Mn oxide precipitation or a Mn-oxide shuttle to the sediment-seawater interface may be linked to the
121 presence of an oxygenated water column [11, 31]. Although the sedimentary and diagenetic pathways
122 responsible for the incorporation of Mn into IFs has recently been questioned [32], secular trends in the
123 relative enrichment of Mn in IFs are typically tied to marine redox conditions. Therefore, as IFs serve as
124 robust archives of both the Fe isotope and Mn/Fe ratios in the deep time, they may be interrogated to
125 constrain the redox state of local seawater during IF deposition. Importantly, a coupled approach such as
126 this can provide new insights into the presence of free O_2 in seawater which, in turn, argues against possible
127 anaerobic pathways capable of oxidizing Mn(II) [33, 34]. Such insights are strengthened when a correlation

between these two parameters exists. That is to say, these coupled records are capable of tracking the timing and the evolution, of O_2-driven Fe(II) and Mn(II) oxidation across Earth's history.

Tracking Iron Oxidation with Iron Isotopes

Here, we present a detailed record of bulk-rock Fe isotopes (reported as the ratio of $^{56}Fe/^{54}Fe$, relative to the IRMM-014 reference material standard in parts per thousand; $\delta^{56}Fe$) and Mn/Fe ratios from Archean to early Paleoproterozoic IFs in order to explore the redox dynamics of the early Earth. Data derived from ~770 individual samples include both new results (n = 253) and those obtained from a comprehensive literature survey (n = 517). Samples were passed through a series of strict filters to select for IFs that are most likely to retain a seawater signature (see *Supplementary Materials*). Nearly all samples have a negligible detrital component (< 0.5 wt.% Al_2O_3) and there exists no significant correlation between the paleoredox data ($\delta^{56}Fe$ values and Mn/Fe ratios) and detrital indicators (e.g., Al_2O_3, Table S3), suggesting that secular variations in redox indicators were not driven by detrital input. The predominance of positively fractionated Fe isotope values in IFs is supportive of genetic models, which invoke precipitation of primary Fe(III)-oxyhydroxide minerals [26], as opposed to primary Fe-silicate minerals [12, 23]. Indeed, a recent evaluation of triple Fe isotope systematics in Neoarchean to Paleoproterozoic IF and pyrite samples, indicates that the Neoarchean would have been characterized by a significant oxidized Fe sink prior to the GOE [35]. Aside from being consistent with the Fe isotopic record, the requirement of extensive Fe oxidation is supported by a recent model that has challenged whether post-depositional groundwater flow could have oxidized a significant volume of Fe(II) on reasonable time scales [36]. Therefore, we suggest that IF Fe isotope systematics are consistent with the interpretation that the marine biosphere, namely Fe-oxidizing bacteria (e.g., photoferrotrophs or cyanobacteria), were involved in the oxidation of Fe(II) and the subsequent deposition of IFs. Importantly, Fe isotope data also suggest that secular changes may present a valuable tool for tracking changes in the relative importance of the mechanisms underlying marine Fe(II) oxidation.

To facilitate the discussion of our data, we have split the deposition of IFs into five stages based upon secular variations in their $\delta^{56}Fe$ values and Mn/Fe ratios (Fig. 1). Although these bins did not emerge from a robust statistical treatment of the data, this binning helps illustrate that there are fundamental shifts in the

redox evolution of Earth's early seawater and atmosphere. Stage 1 extends from the Eoarchean into the Paleoarchean (>3.3 Ga) and is characterized by highly positive $\delta^{56}Fe$ values (Fig. 1a), likely the product of deposition under oxygen-limited conditions that favored the partial oxidation of a relatively large marine reservoir of aqueous Fe(II). Also characterized by low Mn/Fe ratios (<0.01) (Fig. 1b), Stage 1 IFs reflect deposition in an anoxic ocean-atmosphere system. This is consistent with evidence from the sedimentary sulfur isotope record, namely the mass-independent fractionation of sulfur isotopes (MIF-S), which is the prevailing geochemical index for an anoxic atmosphere [1, 37]. Accordingly, the oxidation of Fe(II) that facilitated IF genesis during Stage 1 was likely photoferrotrophy [24].

Compared to Stage 1, IFs deposited during Stage 2 (3.3 to 2.8 Ga) are characterized by lower $\delta^{56}Fe$ values (Fig. 1a), suggesting either a greater degree of anoxygenic photosynthetic Fe(II) oxidation [38] or elevated marine O_2 concentrations. In conjunction with higher Mn/Fe ratios in Stage 2 IFs (Fig. 1b), we propose that the transition to Stage 2 coincides with the emergence and/or increased impact of oxygenic photosynthesis, implying that free O_2-driven Fe(II) oxidation has been active since ~3.3 Ga. Stage 2 encompasses the deposition of four successions suggested to preserve evidence of pre-GOE O_2 oases (i.e. oxygenated shallow seawater)—the 3.2 Ga Fig Tree and Moodies groups in the Barberton Greenstone Belt [39, 40], the 2.95 Ga Sinqeni Formation in the Pongola Supergroup [11], and the 2.94 Ga Red Lake Greenstone Belt. The data from Moodies and Sinqeni IFs also feature a significant negative correlation between Mn/Fe ratios and $\delta^{56}Fe$ values (Fig. S1), supporting the interpretation that free O_2 began to accumulate in shallow-marine settings during this interval, allowing for Mn(II) oxidation. In the presence of such a shallow-water oxic zone, photoferrotrophs would still have thrived, growing at depth near the base of the photic zone [41]. This would allow photoferrotrophs a preferential access to upwelling nutrients owing to their adaption to lower light levels, thus limiting proliferation of cyanobacteria in the surface ocean [42] and confining cyanobacteria to very near-shore environments where there may have been nutrient input from emergent continents. Further, cyanobacteria expansion would have been held in check by the high Fe(II) concentrations in the upwelling currents because of the oxidative stress resulting from reactions between Fe(II) and O_2 [43]. Indeed, marginalization of cyanobacteria to shallow waters is consistent with limited O_2 production in the Mesoarchean ocean, as evidenced by nitrogen (N) isotopes from shales in the Pongola Supergroup [44] and

the lack of a correlation between $\delta^{56}Fe$ values (up to 1.5‰) and Mn/Fe ratios within the Red Lake banded IF (BIF) (Fig. S1), implying that the redoxcline remained likely above the photic zone. Therefore, the contribution of microaerophilic and nitrate-reducing Fe(II)-oxidizers to Fe cycling [45] during this stage is considered to be minor. Moreover, while a sharp redox boundary between deep and shallow waters was proposed to exist at the depositional site of IFs from the 3.2 Ga Fig Tree Group [40], subsequent studies have reported the frequent occurrence of highly positive $\delta^{56}Fe$ values for these IFs [46, 47], likely supporting either partial Fe(II) oxidation in a reducing oceanic environment [46, 47] or heterogeneity in ocean redox conditions [27]. It is noted that the ~2.95 Ga granular IF (GIF) in the upper Nconga Formation of the Pongola Supergroup possesses positive $\delta^{56}Fe$ values and low Mn/Fe ratios [48]. These features are in stark contrast with those observed in the O_2 oases described above, implying that anoxic conditions were prevalent, disrupted by the presence of spatially restricted disequilibrium between the surface oxygenated oceans and reducing atmosphere [49]. To this end, the 3.22 Ga Moodies Group also records depleted C and enriched N isotopes that suggest an oxidative biogeochemical cycle in a terrestrial environmental [39], consistent with O_2 having been present in local environments near shallow marine oases.

The Fe isotopes and Mn/Fe ratios of IFs deposited during Stage 3 (~2.8-2.5 Ga) are comparable with those of Stage 1 (Fig. 1). Transient and spatially restricted oxygenation events have also been suggested to occur during this interval based on a wide range of geochemical proxies [10, 50, 51]. It also needs to be noted that sulfur-rich exhalites in the ~2.7 Ga Abitibi greenstone belt possess highly negative Fe isotope and higher Mn contents, suggesting the presence of O_2 in the upper part of the water column [52]. However, the IF data presented here do not record evidence of oxygenation events, likely due to either sampling bias or the relatively deep-water depositional environments (below storm wave base) of these IFs. Nevertheless, these samples are from fifteen separate, geographically widespread successions (see *Supplementary Materials*), and are thus considered to be fairly representative of this time interval. The common occurrence of positive $\delta^{56}Fe$ values indicates partial Fe(II) oxidation, coupled with lower Mn/Fe ratios, indicating the widespread presence of fully anoxic conditions. These conditions likely existed in the upper water column with photoferrotrophs being the dominant force in driving Fe(II) oxidation. There is no clear relationship between $\delta^{56}Fe$ values and Mn/Fe ratios during this stage (Fig. S1), further confirming the absence of free O_2 in the

water column. A lack of discrete oxygen oases during this period—as suggested by our data—is further consistent with an Archean world characterized by low levels of primary productivity [53, 54].

Stage 4, from 2.5 to 2.4 Ga, is represented by the most laterally extensive deposition of IFs in Earth history [17], and is immediately preceded by a "whiff" of oxygen at 2.5 Ga [9, 55]. The most striking feature in this interval is that δ^{56}Fe values and Mn/Fe ratios have substantially decreased and increased, respectively, marking the gradual transition of the dominant IF oxidant from photoferrotrophs to free O_2 (Fig. 1). Specifically, for the coeval and correlative Transvaal (South Africa) and Hamersley (Western Australia) basins, continuous IF records and precise geochronological constraints reveal a clear trend for these proxies (Fig. S9 and S12). This trend reflects changing marine redox conditions across large portions of the continental margins worldwide. The δ^{56}Fe values in IFs become more negative towards the latter stage of Stage 4, while Mn/Fe ratios become higher. Significantly, negative correlations between Mn/Fe ratios and δ^{56}Fe values are observed for all IF samples (Fig. S2). We suggest that this is the product of gradually increasing O_2 levels within seawater, whereby the negative δ^{56}Fe values are linked to a progressive distillation during the drawdown of the Fe(II) reservoir [31, 56], resulting in a ^{56}Fe-depleted seawater reservoir. A microbially driven benthic Fe shuttle [57]—which preferentially releases light Fe isotopes—may have also contributed to this isotopically depleted Fe(II) reservoir [27, 58] (see *Supplementary Materials* for a detailed discussion). In either case, these Fe isotope data are compatible with a scenario in which near-complete Fe(II) oxidation is occurring at the redox boundary of a stratified water column [25]. This suggests that by Stage 4, substantial O_2 had started to accumulate in the surface ocean, permitting the development of a stable redoxcline separating deep anoxic and shallow oxygenated seawater. This is consistent with an increasingly important role of free O_2 via oxygenic photosynthesis in oxidizing Fe(II). In addition, there is also a decline in the magnitude of positive europium (Eu) anomalies, a high-temperature hydrothermal indicator of Fe input, during Stage 4 IFs (Fig. S3). When combined with increasing oxidation, wanning hydrothermal Fe input could have contributed to falling Fe(II) levels in seawater, which in turn, would have alleviated Fe toxicity issues for cyanobacteria [43]. Collectively, these events would accelerate the expansion and proliferation of cyanobacteria [42], finally giving rise to well-oxygenated surface seawater. Greater O_2 availability could also have benefited microaerophilic and nitrate dependent Fe(II)-oxidizers [45]. Further, a progressive and

pervasively oxygenated surface seawater layer would also imply some degree of free O_2 accumulation in the atmosphere assuming gas-water exchange equilibrium. Such equilibrium would be fully consistent with geochemical proxy records for oxidative weathering (e.g., chromium abundance, S isotopes) in rocks since ~2.5 Ga [8, 59, 60]. At this stage MIF-S signals are still preserved in sedimentary sulfides, although there is an intriguing possibility that the MIF-S signal was intermittent during this period[5, 8, 60].

Stage 5 corresponds with the permanent loss of MIF-S signals between 2.4 and 2.3 Ga, which effectively constrains the full expression of the GOE [5, 7, 61]. This stage is defined by rare IF deposition and low Mn/Fe ratios (Fig. 1b). We suggest that this reflects the transition from Fe-rich to Fe-poor oceans. This could be linked to either the large-scale oxidative drawdown of the marine Fe(II) reservoir as evidenced by the burial of the giant IF deposits of South Africa and Western Australia, and Fe isotope systematics indicative of Rayleigh fractionation of a significantly diminished Fe(II) pool at the end of Stage 4, or waning hydrothermal Fe(II) input, as shown by weakly positive Eu anomalies observed in the Stage 5 IFs (Fig. S3). The studied IFs and ironstones, for the first time, display a narrow and restricted range of $\delta^{56}Fe$ values, which are indistinguishable from those of bulk silicate Earth ($-0.5 < \delta^{56}Fe < 0.3$ ‰) [27, 62, 63]. This observation is an expected consequence of essentially quantitative Fe(II) oxidation within a well-oxygenated surface ocean in gas exchange equilibrium with the high-O_2 atmosphere, consistent with other independent estimates for atmospheric pO_2 [64].

Modeling ocean-atmosphere O_2 abundance

In order to quantitatively estimate the dissolved O_2 concentration of the surface ocean and corresponding atmospheric pO_2, we focused on shallow-marine GIFs and ironstones, which feature Fe ooids. In contrast to deep-marine BIFs, these facies were deposited in water depths close to, or above, storm and fair-weather wave base in near-shore environments [16, 17]. This is important because unlike deep-marine settings, shallow seawater is unlikely to be deficient in dissolved O_2 relative to the overlying oxygenated atmosphere. These O_2 oases likely included the 3.2 Ga Fig Tree and Moodies groups[39, 40], the 2.95 Ga Sinqeni Formation [11], and the 2.94 Ga Red Lake Greenstone Belt, and would have been characterized by shallow oxygenated waters set against a backdrop of prevailing anoxic conditions in both the water column and atmosphere.

While oases may have been transient in nature, leading to the generation of 'whiffs' of O_2 [9], modelling has also suggested that they may have been more static and laterally extensive, correlated to areas of high nutrient input or upwelling coastal waters [53]. In either event, these oases would have been characterized by low dissolved O_2 concentrations on the order of 1-10 μmoll/kg [53], which could have supported the oxidation of Fe(II) and correspondent deposition of IFs.

The first appearance of GIFs in the geological record is marked by the ~2.95 Ga Nconga Formation, and followed by the ~2.45 Ga Griquatown and ~2.31 Ga Timeball Hill formations, the latter two spanning a critical interval pertinent to the GOE. The Fe isotope composition of these facies show a progression through time from positive δ^{56}Fe values, to a mixture of both positive and negative values, to values negligibly fractionated from bulk silicate Earth (Fig. 1a). Therefore, these facies record a marked shift from partial to quantitative Fe(II) oxidation in shallow seawater around ~2.4 Ga. Assuming gas exchange equilibrium and given that nearly all of Fe in the latter two facies were oxidized ultimately by free O_2, partial Fe(II) oxidation in shallow seawater represents robust evidence for low atmospheric pO_2, whereas quantitative Fe(II) oxidation indicates comparatively higher pO_2. We can use a Rayleigh distillation model (see *Supplementary Materials*) to invert these Fe isotope data for an estimate of the extent of Fe(II) oxidation (Fig. 2a). The results show a statistically significant difference between the Griquatown GIF and Timeball Hill ironstone, of which the latter exhibits δ^{56}Fe values that we consider as clear evidence for complete Fe(II) oxidation (Fig. 2a). We can then combine these observations with a statistical model of Fe(II) oxidation kinetics taking into account a wide range of possible marine pH values, surface water temperatures, and variable residence times of water masses within the shallow ocean (see *Supplementary Materials*). We find that the Fe isotope signatures observed in the Timeball Hill ironstone are extremely difficult to explain unless the dissolved O_2 concentration of their contemporaneous shallow seawater was above 5 μmol/kg, corresponding to atmospheric pO_2 above ~1-2% PAL. Further, partial Fe(II) oxidation responsible for the deposition of the Griquatown GIF most likely requires dissolved O_2 and atmospheric pO_2 below 1 μmol/kg and ~0.1-0.5% PAL, respectively (Fig. 2b). We also invert the Fe isotope data of those BIFs deposited in Archean-early Paleoproterozoic ocean oases for estimating dissolved O_2 concentration

of the photic zone (Fig. 2 and S14). We show that dissolved O_2 was below 1 μmol/kg except for the ~2.34 Ga photic zone where levels rose above 5 μmol/kg O_2.

Our results strongly support a dominantly anoxic world before ~2.4 Ga with local oxygen oases containing < 1 μmol/kg O_2, broadly consistent with previous modeling results for a typical O_2 concentration (1-10 μmol/kg O_2) within an Archean oasis [53, 54]. Given that a dissolved O_2 concentration of 1 μmol/kg is equivalent to a roughly 500-fold oversaturation with respect to an atmospheric pO_2 of ~10^{-5} PAL (Fig. 2b), it is reasonable to imagine severe ocean-atmosphere disequilibrium with respect to O_2 on a reducing Archean Earth surface within biologically productive regions of the ocean. Assuming that the carbon export flux from the photic zone was dominated by oxygenic photosynthesis in local oases, such a low O_2 state necessitates that net primary productivity be significantly lower than that of equivalent modern environments, especially given the expectation of increased carbon burial efficiency during the Archean [65].

As the export flux can also be expected to respond to rates of primary productivity, which are in turn limited by the recharge of nutrients (e.g., phosphorus (P) and N), low dissolved O_2 concentrations require sustained low nutrient conditions prior to ~2.4 Ga. For instance, mass balance considerations have shown that for the Proterozoic, depressed net primary productivity, driven by P limitation, is necessary to maintain a low oxygen state [65]; there is no reason to expect that this should be different prior to the GOE. If P is considered to be the nutrient ultimately controlling marine primary productivity in the Archean and early Paleoproterozoic oceans [66], there should be a clear difference with respect to the oceanic inventory of P before and after ~2.4 Ga. A subtle distinction in this regard, is the difference between the overall size of the P reservoir through time and how much is available or accessible to the biosphere. While IFs have provided evidence for a sizeable P reservoir [67], the record of shallow marine environments stands in stark contrast suggesting that P limitation characterized much of Earth's history [68]. This difference may reflect the enhanced sequestration of P by Fe-phases (oxides, green rusts, viviantie) [68], or the limited recycling of P during biomass remineralization [69]. In either event, this would have limited the P available to primary producers in shallow waters and imposed a direct effect on the degree of primary productivity and, by extension, O_2 production. Based on previous Earth system model simulations [53], the predominantly anoxic

surface ocean implies that the oceanic P inventory of the Archean may have been as low as 25% of the modern, whereas P levels similar to, or higher than, the modern may have resulted in the establishment of a well-oxygenated surface ocean at ~2.31 Ga.

Conclusions

In sum, our findings provide new and complementary insights into how the redox structure of the ocean and atmosphere varied through the Archean to early Paleoproterozoic (Fig. 3). Coupled Fe isotope and Mn/Fe ratio data in IFs extend the first production and local accumulation of O_2 in the ocean to at least the latest Paleoarchean, and, when viewed in light of MIF-S signals [46], further confirm that oxygenic photosynthesis was active well before the first permanent oxygenation of the atmosphere during the GOE and that free O_2 produced via oxygenic photosynthesis started to play a role in regulating the oxidation of marine Fe(II) since ~3.3 Ga. However, despite the early presence of cyanobacteria, they probably had no critical direct effect on marine Fe cycling initially, and photoferrotrophy remained the dominant mechanism for Fe(II) oxidation in the Archean ocean, as oxygenated shallow seawater oases in the Archean were transient and spatially restricted.

Importantly, our results argue for a pervasive oxygenation of the shallow ocean during the GOE, with dissolved O_2 concentrations in surface ocean increasing from below 1 to at least 5 μmol/kg. This clearly marks the revolutionary and progressive transition of the dominant oxidative mechanism of marine Fe(II) from photoferrotrophy to free O_2 produced via cyanobacteria at this time. Such a transition could have been closely linked to the growing degree of net primary productivity in the marine environments, ultimately contributing to the progressive, and permanent, oxidation of Earth's surface oceans and atmosphere.

Materials and Methods

IF samples were collected from surface outcrop and drill holes and prepared as polished thin sections and analyzed using reflected light microscopy, Raman spectroscopy, and scanning electron microscopy. Well-preserved IF samples were crushed in an agate mill to a fine powder, and sample powders were digested for bulk rock geochemical analyses. Major and trace element compositions were determined using an

inductively coupled plasma-mass spectrometer (ICP-MS). For Fe isotope analysis, Fe was purified from sample solutions using ion-exchange chromatography and measured using a multi-collector ICP-MS. Refer to *Supplementary Materials* for detailed methods. All data discussed in the paper are included in Supplementary Tables S1–S2.

375

376

377 **Figures**

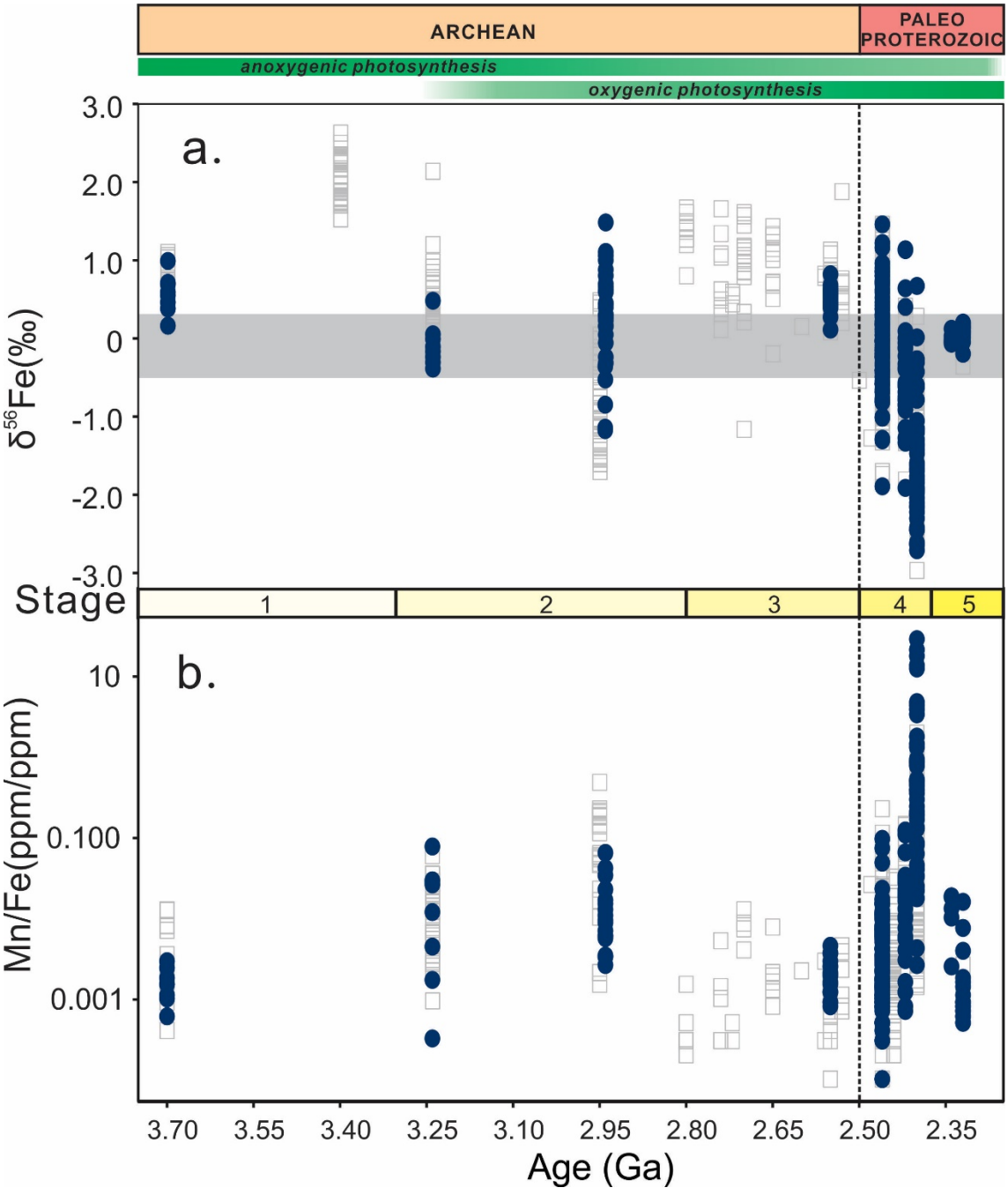

378

379 **Fig. 1.** Temporal variations in $\delta^{56}Fe$ values (a) and Mn/Fe ratios (b) of bulk Archean and Paleoproterozoic
380 iron formations, ferruginous cherts, and ironstones. Filled blue circles represent new results; unfilled gray
381 squares indicate previous results. Detailed sources of these data are provided in the *Supplemental*

Materials. Sample standard error is smaller than the data points. Horizontal gray bar denotes the range of $\delta^{56}Fe$ values of lithogenic and hydrothermal Fe(II) sources ($-0.5 < \delta^{56}Fe < 0.3$ ‰) [27, 62, 63]. Note the logarithmic scale in (b).

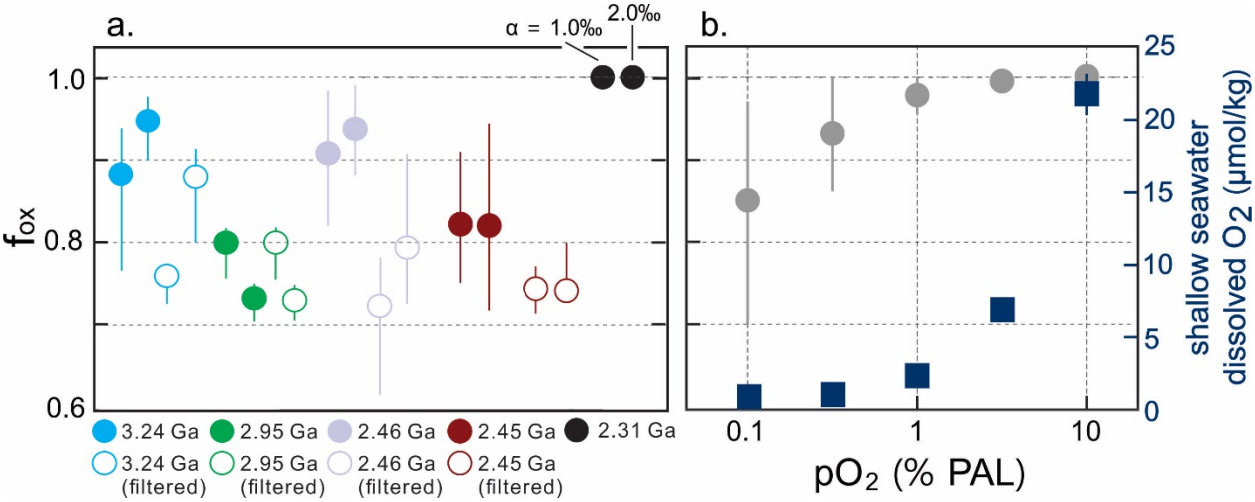

Fig. 2. A model for Fe(II) oxidation in the ~3.24 Ga Moodies BIF, ~2.95 Ga Sinqeni BIF, ~2.46 Ga BIFs in western Australia and South Africa, ~2.45 Ga Griquatown GIF, and ~2.31 Ga Timeball Hill ironstone as a function of dissolved O_2 abundance of the surface ocean or photic zone. Shown in (a) are estimates of the fraction of Fe(II) oxidized in shallow marine environments (f_{ox}) based on a Rayleigh distillation model assuming two overall isotope effects (α = 1.0 (left) and 2.0‰ (right)) for the combined processes of Fe(II) oxidation and precipitation as Fe(III)-(oxyhydr)oxides (see *Supplementary Materials*). Results are shown for the combined data (filled circles) and data filtered to exclude non-fractionated samples (open circles). Error bars show ±1σ for the entire subsampled dataset. Shown in (b) are results from a kinetic model of Fe(II) oxidation, resampled 10,000 times at each atmospheric pO_2 value (relative to PAL) across a range of seawater pH and temperature values. Note that every pO_2 value corresponds to one shallow seawater dissolved O_2 concentration (μmol/kg) assuming gas-water exchange equilibrium. Error bars show ±1σ. Also note that partial Fe oxidation during the Archean is indicative of low net primary productivity. The systematics of the observed ~2.45 Ga samples are difficult to explain unless dissolved O_2 and atmospheric pO_2 were below 1 μmol/kg and ~0.1 % PAL, respectively, while the ~2.31 Ga Timeball Hill data imply dissolved O_2 at least 5 μmol/kg and a minimum atmospheric pO_2 of ~1% PAL during GOE.

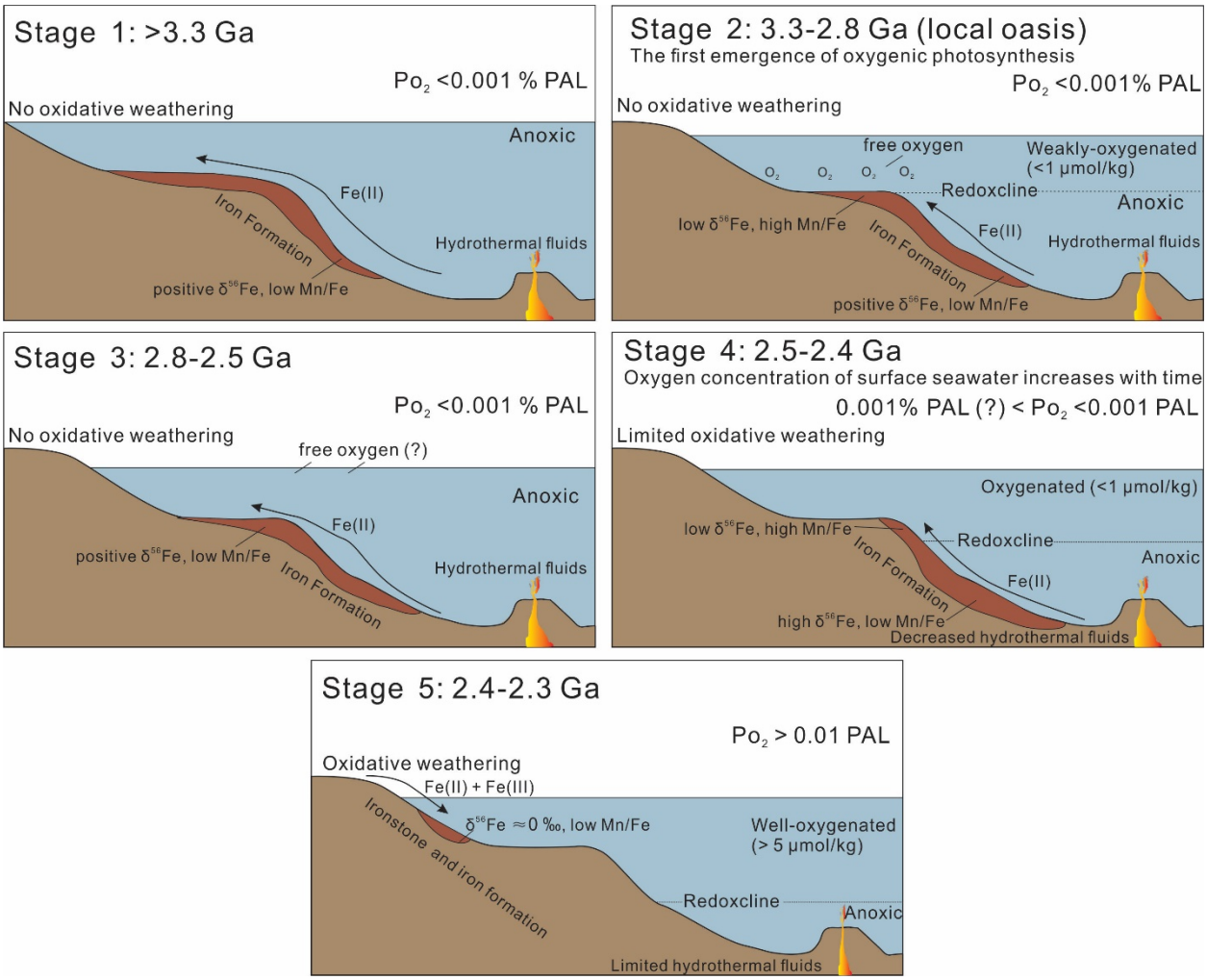

Fig. 3. Schematic diagram showing the temporal progression of oxygenation of the Archean to early Paleoproterozoic ocean and atmosphere.

ACKNOWLEDGMENTS: The manuscript benefitted from discussions with Andrey Bekker. We also acknowledge Xuefang Wu for helping to measure Fe isotopes and Andrey Bekker for providing the Timeball Hill samples. **Funding:** This work was supported by grants from the Key Research Program of the Institute of Geology and Geophysics, CAS (grant IGGCAS-201905), National Natural Science Foundation of China (grant 41872087 and 41890833), Youth Innovation Promotion Association, Chinese Academy of Sciences, and China Scholarship Council to C.L.W. S.V.L. and L.A.P. acknowledge support from the European Union's Horizon 2020 research and innovation programme (grant agreement no 716515 to S.V.L.). **Author contributions:** C.L.W. and N.J.P. conceived the study. C.L.W. processed the samples. C.L.W. and D.A. conducted geochemical analyses. C.L.W., N.J.B., S.V.L., L.C.Z., and K.O.K. collected samples for this study. L.A.P. provided additional new data for Red Lake samples. N.J.P. and C.T.R. are responsible for the iron oxidation calculations. All authors contributed to writing and editing the manuscript. **Competing interests:** The authors declare no competing interests. **Data and materials availability:** All data used in the paper are either tabulated in the Supplementary Materials or published in the cited references.

References

1. Farquhar J, Zerkle AL, Bekker A. Geological constraints on the origin of oxygenic photosynthesis. *Photosynthesis research* **107**, 11-36 (2011).

2. Lyons TW, Reinhard CT, Planavsky NJ. The rise of oxygen in Earth's early ocean and atmosphere. *Nature* **506**, 307-315 (2014).

3. Bekker A*, et al.* Dating the rise of atmospheric oxygen. *Nature* **427**, 117-120 (2004).

4. Canfield DE. The early history of atmospheric oxygen: homage to Robert M. Garrels. *Annu Rev Earth Planet Sci* **33**, 1-36 (2005).

5. Guo Q*, et al.* Reconstructing Earth's surface oxidation across the Archean-Proterozoic transition. *Geology* **37**, 399-402 (2009).

6. Holland HD. The oxygenation of the atmosphere and oceans. *Philosophical Transactions of the Royal Society B: Biological Sciences* **361**, 903-915 (2006).

7. Luo G, Ono S, Beukes NJ, Wang DT, Xie S, Summons RE. Rapid oxygenation of Earth's atmosphere 2.33 billion years ago. *Science Advances* **2**, e1600134 (2016).

8. Warke MR*, et al.* The Great Oxidation Event preceded a Paleoproterozoic "snowball Earth". *Proceedings of the National Academy of Sciences*, (2020).

9. Anbar AD*, et al.* A whiff of oxygen before the Great Oxidation Event? *Science* **317**, 1903-1906 (2007).

10. Koehler MC, Buick R, Kipp MA, Stüeken EE, Zaloumis J. Transient surface ocean oxygenation recorded in the~ 2.66-Ga Jeerinah Formation, Australia. *Proceedings of the National Academy of Sciences* **115**, 7711-7716 (2018).

11. Planavsky NJ*, et al.* Evidence for oxygenic photosynthesis half a billion years before the Great Oxidation Event. *Nature Geoscience* **7**, 283-286 (2014).

12. Rasmussen B, Muhling JR, Tosca NJ, Tsikos H. Evidence for anoxic shallow oceans at 2.45 Ga: Implications for the rise of oxygenic photosynthesis. *Geology* **47**, 622-626 (2019).

13. Soo RM, Hemp J, Hugenholtz P. The evolution of photosynthesis and aerobic respiration in the cyanobacteria. *Free Radical Biology and Medicine*, (2019).

14. Fischer WW, Hemp J, Johnson JE. Evolution of oxygenic photosynthesis. *Annual Review of Earth and Planetary Sciences* **44**, 647-683 (2016).

15. Jabłońska J, Tawfik DS. The evolution of oxygen-utilizing enzymes suggests early biosphere oxygenation. *Nature Ecology & Evolution*, 1-7 (2021).

16. Bekker A*, et al.* Iron Formation: The Sedimentary Product of a Complex Interplay among Mantle, Tectonic, Oceanic, and Biospheric Processes. *Economic Geology* **105**, 467-508 (2010).

17. Konhauser K*, et al.* Iron formations: A global record of Neoarchaean to Palaeoproterozoic environmental history. *Earth-Science Reviews* **172**, 140-177 (2017).

18. Robbins LJ*, et al.* Trace elements at the intersection of marine biological and geochemical evolution. *Earth-Science Reviews* **163**, 323-348 (2016).

19. Cloud P. Paleoecological significance of the banded iron-formation. *Economic Geology* **68**, 1135-1143 (1973).

20. Garrels R, Perry E, Mackenzie F. Genesis of Precambrian iron-formations and the development of atmospheric oxygen. *Economic Geology* **68**, 1173-1179 (1973).

21. Konhauser KO*, et al.* Could bacteria have formed the Precambrian banded iron formations? *Geology* **30**, 1079-1082 (2002).

22. Konhauser KO*, et al.* Phytoplankton contributions to the trace-element composition of Precambrian banded iron formations. *Bulletin* **130**, 941-951 (2018).

23. Muhling JR, Rasmussen B. Widespread deposition of greenalite to form Banded Iron Formations before the Great Oxidation Event. *Precambrian Research* **339**, 105619 (2020).

24. Czaja AD, Johnson CM, Beard BL, Roden EE, Li W, Moorbath S. Biological Fe oxidation controlled deposition of banded iron formation in the ca. 3770 Ma Isua Supracrustal Belt (West Greenland). *Earth and Planetary Science Letters* **363**, 192-203 (2013).

25. Busigny V*, et al.* Iron isotopes in an Archean ocean analogue. *Geochimica et Cosmochimica Acta* **133**, 443-462 (2014).

26. Dauphas N, John SG, Rouxel O. Iron isotope systematics. *Reviews in Mineralogy and Geochemistry* **82**, 415-510 (2017).

27. Johnson C, Beard B, Weyer S. The Ancient Earth. In: *Iron Geochemistry: An Isotopic Perspective* (ed^(eds). Springer (2020).

28. Croal LR, Johnson CM, Beard BL, Newman DK. Iron isotope fractionation by Fe (II)-oxidizing photoautotrophic bacteria. *Geochimica et cosmochimica acta* **68**, 1227-1242 (2004).

29. Johnson C, Beard B, Weyer S. Iron Geochemistry: An Isotopic Perspective. In: *Iron Geochemistry: An Isotopic Perspective* (ed^(eds). Springer (2020).

30. Tebo BM, Johnson HA, McCarthy JK, Templeton AS. Geomicrobiology of manganese (II) oxidation. *TRENDS in Microbiology* **13**, 421-428 (2005).

31. Kurzweil F, Wille M, Gantert N, Beukes NJ, Schoenberg R. Manganese oxide shuttling in pre-GOE oceans–evidence from molybdenum and iron isotopes. *Earth and planetary science letters* **452**, 69-78 (2016).

32. Siahi M*, et al.* Insights into the processes and controls on the absolute abundance and distribution of manganese in Precambrian iron formations. *Precambrian Research* **350**, 105878 (2020).

33. Daye M*, et al.* Light-driven anaerobic microbial oxidation of manganese. *Nature* **576**, 311-314 (2019).

34. Liu W*, et al.* Anoxic photogeochemical oxidation of manganese carbonate yields manganese oxide. *Proceedings of the National Academy of Sciences*, (2020).

35. Heard AW*, et al.* Triple iron isotope constraints on the role of ocean iron sinks in early atmospheric oxygenation. *Science* **370**, 446-449 (2020).

36. Robbins LJ*, et al.* Hydrogeological constraints on the formation of Palaeoproterozoic banded iron formations. *Nature Geoscience* **12**, 558-563 (2019).

37. Farquhar J, Bao H, Thiemens M. Atmospheric influence of Earth's earliest sulfur cycle. *Science* **289**, 756-758 (2000).

38. Czaja AD, Van Kranendonk MJ, Beard BL, Johnson CM. A multistage origin for Neoarchean layered hematite-magnetite iron formation from the Weld Range, Yilgarn Craton, Western Australia. *Chemical Geology*, (2018).

39. Homann M*, et al.* Microbial life and biogeochemical cycling on land 3,220 million years ago. *Nature Geoscience* **11**, 665-671 (2018).

40. Satkoski AM, Beukes NJ, Li W, Beard BL, Johnson CM. A redox-stratified ocean 3.2 billion years ago. *Earth and Planetary Science Letters* **430**, 43-53 (2015).

41. Kappler A, Pasquero C, Konhauser KO, Newman DK. Deposition of banded iron formations by anoxygenic phototrophic Fe (II)-oxidizing bacteria. *Geology* **33**, 865-868 (2005).

42. Jones C, Nomosatryo S, Crowe SA, Bjerrum CJ, Canfield DE. Iron oxides, divalent cations, silica, and the early earth phosphorus crisis. *Geology* **43**, 135-138 (2015).

43. Swanner ED, Mloszewska AM, Cirpka OA, Schoenberg R, Konhauser KO, Kappler A. Modulation of oxygen production in Archaean oceans by episodes of Fe (II) toxicity. *Nature Geoscience* **8**, 126-130 (2015).

44. Ossa FO*, et al.* Limited oxygen production in the Mesoarchean ocean. *Proceedings of the National Academy of Sciences* **116**, 6647-6652 (2019).

45. Melton ED, Swanner ED, Behrens S, Schmidt C, Kappler A. The interplay of microbially mediated and abiotic reactions in the biogeochemical Fe cycle. *Nature Reviews Microbiology* **12**, 797-808 (2014).

46. Busigny V*, et al.* Iron and sulfur isotope constraints on redox conditions associated with the 3.2 Ga barite deposits of the Mapepe Formation (Barberton Greenstone Belt, South Africa). *Geochimica et Cosmochimica Acta* **210**, 247-266 (2017).

47. Planavsky N, Rouxel OJ, Bekker A, Hofmann A, Little CT, Lyons TW. Iron isotope composition of some Archean and Proterozoic iron formations. *Geochimica et Cosmochimica Acta* **80**, 158-169 (2012).

48. Smith A, Beukes N, Gutzmer J, Czaja A, Johnson C, Nhleko N. Oncoidal granular iron formation in the Mesoarchaean Pongola Supergroup, southern Africa: Textural and geochemical evidence for biological activity during iron deposition. *Geobiology* **15**, 731-749 (2017).

49. Eickmann B, Hofmann A, Wille M, Bui TH, Wing BA, Schoenberg R. Isotopic evidence for oxygenated Mesoarchaean shallow oceans. *Nature geoscience* **11**, 133-138 (2018).

50. Czaja AD*, et al.* Evidence for free oxygen in the Neoarchean ocean based on coupled iron–molybdenum isotope fractionation. *Geochimica et Cosmochimica Acta* **86**, 118-137 (2012).

51. Wille M*, et al.* Evidence for a gradual rise of oxygen between 2.6 and 2.5 Ga from Mo isotopes and Re-PGE signatures in shales. *Geochimica et Cosmochimica Acta* **71**, 2417-2435 (2007).

52. Hiebert R, Bekker A, Houlé M, Rouxel O. Depositional setting of the Late Archean Fe oxide-and sulfide-bearing chert and graphitic argillite in the Shaw Dome, Abitibi Greenstone Belt, Canada. *Precambrian Research* **311**, 98-116 (2018).

53. Olson SL, Kump LR, Kasting JF. Quantifying the areal extent and dissolved oxygen concentrations of Archean oxygen oases. *Chemical Geology* **362**, 35-43 (2013).

54. Reinhard CT, Lalonde SV, Lyons TW. Oxidative sulfide dissolution on the early Earth. *Chemical Geology* **362**, 44-55 (2013).

55. Kendall B, Creaser RA, Reinhard CT, Lyons TW, Anbar AD. Transient episodes of mild environmental oxygenation and oxidative continental weathering during the late Archean. *Science advances* **1**, e1500777 (2015).

56. Rouxel OJ, Bekker A, Edwards KJ. Iron isotope constraints on the Archean and Paleoproterozoic ocean redox state. *Science* **307**, 1088-1091 (2005).

57. Severmann S, Lyons TW, Anbar A, McManus J, Gordon G. Modern iron isotope perspective on the benthic iron shuttle and the redox evolution of ancient oceans. *Geology* **36**, 487-490 (2008).

58. Li W, Beard BL, Johnson CM. Biologically recycled continental iron is a major component in banded iron formations. *Proceedings of the National Academy of Sciences* **112**, 8193-8198 (2015).

59. Konhauser KO*, et al.* Aerobic bacterial pyrite oxidation and acid rock drainage during the Great Oxidation Event. *Nature* **478**, 369-373 (2011).

60. Philippot P*, et al.* Globally asynchronous sulphur isotope signals require re-definition of the Great Oxidation Event. *Nature communications* **9**, 1-10 (2018).

61. Bekker A*, et al.* Dating the rise of atmospheric oxygen. *Nature* **427**, 117-120 (2004).

62. Beard BL, Johnson CM, Von Damm KL, Poulson RL. Iron isotope constraints on Fe cycling and mass balance in oxygenated Earth oceans. *Geology* **31**, 629-632 (2003).

63. Severmann S*, et al.* The effect of plume processes on the Fe isotope composition of hydrothermally derived Fe in the deep ocean as inferred from the Rainbow vent site, Mid-Atlantic Ridge, 36 14′ N. *Earth and Planetary Science Letters* **225**, 63-76 (2004).

64. Bekker A, Holland H. Oxygen overshoot and recovery during the early Paleoproterozoic. *Earth and Planetary Science Letters* **317**, 295-304 (2012).

65. Laakso TA, Schrag DP. Limitations on limitation. *Global Biogeochemical Cycles* **32**, 486-496 (2018).

66. Tyrrell T. The relative influences of nitrogen and phosphorus on oceanic primary production. *Nature* **400**, 525-531 (1999).

67. Planavsky NJ*, et al.* The evolution of the marine phosphate reservoir. *Nature* **467**, 1088-1090 (2010).

68. Reinhard CT*, et al.* Evolution of the global phosphorus cycle. *Nature* **541**, 386-389 (2017).

69. Kipp MA, Stüeken EE. Biomass recycling and Earth's early phosphorus cycle. *Science advances* **3**, eaao4795 (2017).